


ABO₃ perovskite as well as BaF₂, SrF₂ and CaF₂ bulk and surface *F*-center first principles predictions

Roberts Eglitis ^{*}, J. Purans , A. I. Popov  and S. Piskunov 

*Institute of Solid State Physics, University of Latvia,
8 Kengaraga Str., Riga LV1063, Latvia
rieglitis@gmail.com

Ran Jia 

*Laboratory of Theoretical and Computational Chemistry,
Institute of Theoretical Chemistry,
Jilin University, Changchun 130023, China
jiaran@jlu.edu.cn*

S. P. Kruchinin 

*Bogolyubov Institute for Theoretical Physics,
NASU, 03143 Kyiv, Ukraine; University of Leipzig,
Felix Bloch Institute for Solid State Physics,
04103 Leipzig, Germany
sergeikruchinin@yahoo.com*

Received 15 April 2023

Accepted 12 October 2023

Published 28 November 2023

We, at the *ab initio* level, simulated the rearrangement magnitudes of the adjacent neighboring ions, surrounding the (100) surface *F*-center in ABO₃ perovskite matrixes. They are noticeably greater than the respective ionic shift magnitudes of the adjacent neighboring ions surrounding the bulk *F*-center. In ABO₃ perovskites, the electron charge is noticeably better bounded on the inside of the bulk oxygen vacancy, as interior the respective (100) surface vacancy. The oxygen vacancy formation energy, located on the (100) surface of ABO₃ perovskites, as a rule, is smaller as in the bulk. This slight energy distinction encourages the oxygen vacancy segregation from the ABO₃ perovskite bulk to their (100) surfaces. The ABO₃ complex oxide (100) surface *F*-center generated defect levels are positioned nearer to the (100) surface CB bottom than the bulk *F*-center generated respective defect levels. In contrary, the BaF₂, SrF₂ and CaF₂, both, surface and bulk *F*-center charges are well localized inside the fluorine vacancy. The ionic rearrangement magnitudes of the adjacent neighboring ions, surrounding the surface and bulk *F*-centers in BaF₂, SrF₂ and CaF₂ matrixes, are much smaller regarding the respective situation in ABO₃ perovskites.

Keywords: *Ab initio* computations; *F*-center; oxygen vacancy; ABO₃ perovskites; defects; BaF₂.

*Corresponding author.

1. Introduction

Different aspects of ABO_3 perovskite (100) surfaces as well as their (100) heterostructures are very hot topics in modern condensed matter physics.^{1–17} $SrTiO_3$ (STO) is frequently utilized for substrates of superconducting thin films.¹⁸ The perfect energy band structure as well as suitable light absorption, combined with increased carrier disconnection of $TiO_2/SrTiO_3$ heterojunction promote the creation of reactive bactericidal oxygen species.¹⁹ $BaTiO_3$ (BTO) is used in multiple technological implementations, for example, as transducers, sensors and multilayer capacitors.^{20–22} Recently, the multilayered $TiO_2/BaTiO_3/Au$ heterostructured nanorod arrangement was successfully synthesized for the improvement of photodynamic work as an antibacterial coating.²³ $PbZrO_3$ perovskite has a huge implementation potential in power generators as well as in energy storage capacitors.²⁴ $SrZrO_3$ complex oxide material is an attractive candidate for a huge variety of optoelectronic applications.²⁵ Barium fluoride (BaF_2) is frequently used as a viewport window for implementations in thermography.²⁶ Strontium fluoride (SrF_2) is an optical material. SrF_2 is used as a thermoluminescent dosimeter crystal as well as the optical coating on lenses.²⁷ Finally, calcium fluoride (CaF_2) is widely used as the flux in the aluminum industry.²⁸

The F -center resonance in CaF_2 matrix has been experimentally detected by Arends²⁹ and well correlated with the optical absorption band located at 3.3 eV. According to experimental measurements performed by Nepomnyashchikh *et al.*,³⁰ the X-ray irradiation of undoped BaF_2 crystal at 77 K temperature creates the F -centers having optical absorption band located at 2.3 eV.³⁰ Lastly, the experimentally detected F -center absorption energy in the SrF_2 matrix at very low 4 K temperature is situated at 2.85 eV.³¹ It is well known that nowadays the defect engineering is a very efficient approach to manipulate the physical properties of different technologically relevant materials.^{32–35} Oxygen vacancy (V_O) in the ABO_3 perovskites traps two electrons.³⁶ V_O is the most frequent classical point defect in the ABO_3 perovskites and it is denoted in the scientific literature as the F -center. The F -center in BaF_2 , SrF_2 and CaF_2 matrixes is a single electron trapped inside the anion vacancy.^{37–39}

Strontium titanate (STO) is the centrosymmetric paraelectric and cubic material at room temperature (RT).⁴⁰ STO has the symmetry group ($Pm\bar{3}m$) and the symmetry group number 221. Exactly the same symmetry group ($Pm\bar{3}m$) as well as the symmetry group number 221 in the cubic phase have also another ABO_3 perovskites, including our studied $BaTiO_3$, $SrZrO_3$ and $PbZrO_3$ matrixes. STO and another our computed ABO_3 perovskites have 5 atoms in the primitive cell.⁴¹ Namely, the Sr ion is located at the corner of the cubic unit cell with the following coordinates (0, 0, 0). The O ions are located at the face centers of the cube with the subsequent coordinates (0.5, 0.5, 0), (0.5, 0, 0.5), (0, 0.5, 0.5). Lastly, the Ti ion is located at the center of the cubic unit cell with the consecutive coordinates (0.5, 0.5, 0.5). Another class of our computed materials SrF_2 , BaF_2 and CaF_2 cubic unit cell contains three atoms.

One cation (Sr, Ba or Ca) is chosen as the coordinate origin in our computations (0, 0, 0) as well as two anions are located at the following coordinates (1/4*a*, 1/4*a*, 1/4*a*) and (3/4*a*, 3/4*a*, 3/4*a*). There *a* is the SrF₂, BaF₂ and CaF₂ bulk lattice constant. All our computed SrF₂, BaF₂ and CaF₂ matrixes are the cubic (*Fm* $\bar{3}$ *m*) large bandgap insulators. All of them have the 225 symmetry group number.⁴² The BaTiO₃ perovskite has several phase transitions. Namely, the BaTiO₃ matrix structure changes⁴³ from rhombohedral (*R*3*m*) structure to orthorhombic (*Amm*2) structure at 183 K temperature. At 278 K temperature, the BaTiO₃ structure changes to tetragonal phase (*P*4*mm*). Finally, at 403 K temperature, the BaTiO₃ structure changes to cubic phase (*Pm* $\bar{3}$ *m*). In the SrZrO₃ perovskite matrix we observed three phase transitions.^{44,45} SrZrO₃ is at orthorhombic phase (*Pnma*) from the room temperature till a temperature of 995 K.^{44,45} From 995 K till 1105 K, SrZrO₃ is in another orthorhombic phase with different symmetry group number (*Cmcm*).^{44,45} From 1105 K till 1440 K temperatures, SrZrO₃ is in the tetragonal phase (*I*4/*mcm*). Finally, at temperatures above 1440 K, SrZrO₃ has the cubic structure with the symmetry group (*Pm* $\bar{3}$ *m*).

The objectives of research, described in this contribution, was to carry out the required additional *ab initio* B3PW computations, in order to finish our long lasting work, dealing with the *F*-centers in PbZrO₃, SrZrO₃, BaTiO₃, SrTiO₃, SrF₂, CaF₂ and BaF₂ matrixes. After finishing our *ab initio* B3PW computations for the *F*-centers in BaTiO₃, SrTiO₃, SrZrO₃, PbZrO₃ perovskites as well as SrF₂, BaF₂ and CaF₂ fluorides, we carefully analyzed systematic tendencies of the *F*-center behavior, and summarized them in a way conveniently accessible for readers.

2. Computational Method

We carried out our first-principles simulations for the *F*-centers in the PbZrO₃, SrZrO₃, BaTiO₃, SrTiO₃ perovskites as well as SrF₂, BaF₂ and CaF₂ fluorides using the brilliant CRYSTAL⁴⁶ computer package. In our numerical simulations, we employed the well-known hybrid exchange-correlation functional B3PW.^{47,48} The world famous CRYSTAL computer program package⁴⁶ utilizes the Gaussian-type basis sets.⁴⁹ In our *ab initio* simulations, each atom in PbZrO₃, SrZrO₃, BaTiO₃, SrTiO₃, SrF₂, BaF₂ and CaF₂ compounds have the localized basis sets.⁴⁶ In our first principles simulations for the SrZrO₃, PbZrO₃, BaTiO₃ and SrTiO₃ perovskites, containing the *F*-center defect, for Sr, Ba, Pb, Ti and O atoms, we employed the basis sets developed by Piskunov *et al.*⁴⁹ Our used atomic basis sets for SrF₂, CaF₂ and BaF₂ matrixes are described in Refs. 37–39. Finally, for the Zr atom, we employed the Zr basis set from the CRYSTAL code home page.⁴⁶ In our *ab initio* computations, we carried out the reciprocal space integration by sampling the Brillouin zone of the PbZrO₃, SrZrO₃, BaTiO₃, SrTiO₃, SrF₂, BaF₂ and CaF₂ unit cell by the 8 × 8 × 8 times expanded Pack-Monkhorst⁵⁰ mesh. We performed bulk *F*-center *ab initio* computations in SrZrO₃, PbZrO₃, BaTiO₃ and SrTiO₃ matrixes employing the 3 × 3 × 3 times expanded supercells containing 135 atoms (Fig. 1).

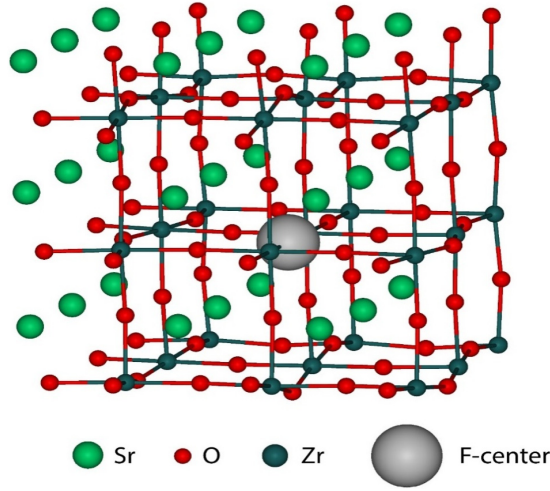


Fig. 1. (Color online) Depiction of our computed SrZrO₃ cubic supercell, with $3 \times 3 \times 3$ extension, containing the *F*-center.

Thereby, in our *ab initio* bulk *F*-center computations in ABO₃ perovskites, the supercell consisted from 134 atoms as well as the single *F*-center (Fig. 1).

In order to simulate the *F*-center, located on the ZrO₂-terminated SrZrO₃ (001) surface (Fig. 2), we used the two-dimensional slab model, which contained 11 layers.⁵¹ In our *ab initio* ZrO₂-terminated SrZrO₃ (001) surface *F*-center simulations, we employed the $3 \times 3 \times 1$ times expanded surface supercells. For SrZrO₃, PbZrO₃ and SrTiO₃ perovskites, we computed the *F*-center located on ZrO₂ or TiO₂-terminated (001) surfaces. In contrast, for the BaTiO₃ matrix, we computed the *F*-center located on the BaO-terminated (001) surface (Fig. 3).⁵² For the *F*-center computations, located on the BaO-terminated BTO (001) surface, we

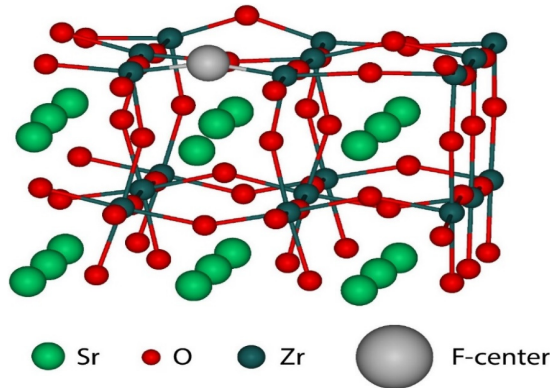


Fig. 2. (Color online) Depiction of the single *F*-center containing ZrO₂-terminated SrZrO₃ (001) surface atomic structure.

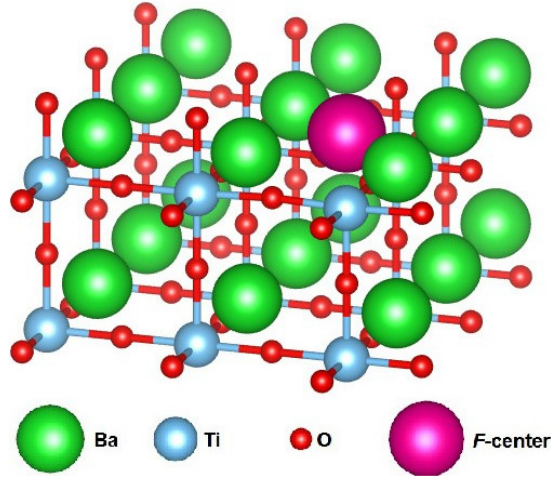


Fig. 3. (Color online) Depiction of the single *F*-center containing BaO-terminated BaTiO₃ (001) surface atomic structure.

used the $3 \times 3 \times 1$ extension of the BTO (001) surface supercells. Our computed BTO (001) slab consisted from 11 layers. Thereby, in our *ab initio* computations, we employed the BTO slab consisting of 242 atoms as well as the single *F*-center, positioned on the BaO-terminated BaTiO₃ (001) surface (Fig. 3).^{52–55} In order to compute the *F*-center defect, we used the 48-atom CaF₂ supercell (Fig. 4). We removed one of the fluorine atoms in the CaF₂ matrix, as depicted in Fig. 4. As a

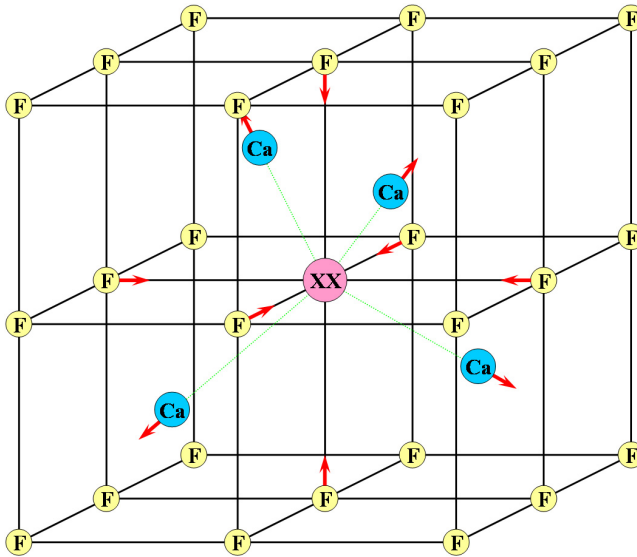


Fig. 4. (Color online) Depiction of the single *F*-center (XX) in the CaF₂ matrix and its nearest neighbor surrounding atoms.

next step, we added the basis set centered at the fluorine vacancy in the CaF_2 matrix, corresponding to the so-called “ghost” atom. This allows to obtain as good as possible description of the F -center in CaF_2 , SrF_2 and BaF_2 matrixes.

3. *Ab initio* Computation Results

As a starting point of our *ab initio* B3PW computations, we computed the SrZrO_3 , BaTiO_3 , PbZrO_3 and SrTiO_3 perovskite as well as BaF_2 , SrF_2 and CaF_2 fluoride bulk lattice constants. Our *ab initio* B3PW computed SrZrO_3 bulk lattice constant (a_0) 4.163 Å is almost in a perfect agreement with the experimentally at 1423 K temperature measured SrZrO_3 cubic structure lattice constant 4.154 Å.⁵⁶ Also, our *ab initio* B3PW computed BaTiO_3 bulk lattice constant 4.007 Å is in a fine agreement with the experimentally measured BaTiO_3 lattice constant in a cubic phase equal to 4.00 Å.⁵⁷ The same, also our *ab initio* B3PW computed PbZrO_3 bulk lattice constant, equal to 4.177 Å, is in a fair agreement with the experimentally detected respective PbZrO_3 lattice constant in a cubic phase, measured at 520 K temperature — 4.1614 Å.⁵⁸ Finally, our *ab initio* B3PW computed SrTiO_3 bulk lattice constant 3.904 Å is in almost ideal coincidence with the experimentally measured SrTiO_3 lattice constant in the cubic structure equal to 3.89845 Å at 110 K temperature⁵⁹ (Table 1). Also, for BaF_2 , SrF_2 and CaF_2 fluorides, our *ab initio* B3PW computed bulk lattice constants (6.26 Å, 5.845 Å and 5.50 Å, respectively) are in a good agreement with the available experimental data (6.20 Å,⁶⁰ 5.799 Å,⁶¹ 5.46 Å,⁶² respectively) (Table 1).

Our *ab initio* B3PW computed SrZrO_3 bulk Γ - Γ bandgap is equal to exactly 5.00 eV for the pristine SrZrO_3 crystal, whereas the *ab initio* computed SrZrO_3 Γ - Γ bulk bandgap for the F -center defect containing SrZrO_3 crystal is slightly larger and equal to 5.07 eV. The experimentally measured SrZrO_3 bulk Γ - Γ band gap is available only in the orthorhombic phase (5.6 eV),⁶³ stable at RT. Our *ab initio* B3PW computed BaTiO_3 bulk Γ - Γ bandgap is equal to 3.55 eV (Table 2). The single F -center defect containing BaTiO_3 bulk Γ - Γ bandgap is slightly larger (3.58) eV. According to the experiments, performed by Wemple,⁶⁴ BaTiO_3 bulk Γ - Γ bandgap at RT is equal to 3.38 or 3.27 eV for light polarized parallel or perpendicular, respectively, to the ferroelectric axis c . Our *ab initio* B3PW computed PbZrO_3 bulk X-X bandgap is equal to 3.79 eV. It is in good agreement with the experimentally detected⁶⁵ PbZrO_3 bandgap in the RT at orthorhombic phase 3.7 eV.⁶⁵ The B3PW

Table 1. *Ab initio* B3PW computed and experimental SrZrO_3 , BaTiO_3 , PbZrO_3 , SrTiO_3 , BaF_2 , SrF_2 and CaF_2 bulk lattice constants (in Å).

Material	SrZrO_3	BaTiO_3	PbZrO_3	SrTiO_3	BaF_2	SrF_2	CaF_2
Functional Theory	B3PW 4.163	B3PW 4.007	B3PW 4.177	B3PW 3.904	B3PW 6.26	B3PW 5.845	B3PW 5.50
Experiment	4.154 Ref. 56	4.00 (Ref. 57)	4.1614 (Ref. 58)	3.89845 (Ref. 59)	6.20 (Ref. 60)	5.799 (Ref. 61)	5.46 (Ref. 62)

Table 2. *Ab initio* B3PW computed and experimental SrZrO₃, BaTiO₃, PbZrO₃, CaF₂, BaF₂ and SrF₂ as well as F-center defect containing bulk bandgaps (in eV).

Material	SrZrO ₃	BaTiO ₃	PbZrO ₃	CaF ₂	BaF ₂	SrF ₂
Bandgap	5.00	3.55	3.79	10.96	11.30	11.31
Gap with F-center	5.07	3.58	3.97	10.99	11.28	11.34
Experiment	5.6 (Ref. 63) (Orthorhombic phase)	3.38; 3.27 (Ref. 64) (Tetragonal ↔ Orthorhombic)	3.7 (Ref. 65) (Orth. Phase)	12.1 (Ref. 66)	11.00 (Ref. 66)	11.25 (Ref. 66)

computed X-X band gap for PbZrO₃ bulk, containing the F-center defect, is equal to 3.97 eV (Table 2). Our *ab initio* B3PW computed bulk Γ - Γ bandgap value for CaF₂ (10.96 eV) is by 1.14 eV underestimated regarding the experimental value (12.1 eV)⁶⁶ (Table 2). The Γ - Γ bulk bandgap for the CaF₂ fluoride, containing the F-center defect, is equal to 10.99 eV (Table 2). The B3PW computed BaF₂ bulk bandgap at Γ -point is equal to 11.30 eV, whereas the bandgap at the same Γ -point for BaF₂ fluoride containing the F-center defect is equal to 11.28 eV. The experimentally measured BaF₂ direct bandgap at Γ -point is equal to 11.00 eV.⁶⁶ Finally, our *ab initio* B3PW computed SrF₂ bulk Γ - Γ bandgap is equal to 11.31 eV, whereas the bandgap for the SrF₂ matrix containing the F-center is larger by 0.03 eV and equal to 11.34 eV. The experimental SrF₂ optical bulk band gap is equal to 11.25 eV,⁶⁶ almost in a perfect agreement with our *ab initio* B3PW computation result.

As we can see from the Table 2 and Fig. 5, our *ab initio* B3PW computed SrZrO₃, BaTiO₃, PbZrO₃, CaF₂, BaF₂ and SrF₂ bulk bandgaps always are in a fair agreement with the available experimental data. The largest difference between our *ab initio* B3PW computed CaF₂ bulk Γ - Γ bandgap (10.96 eV) as well as experimentally

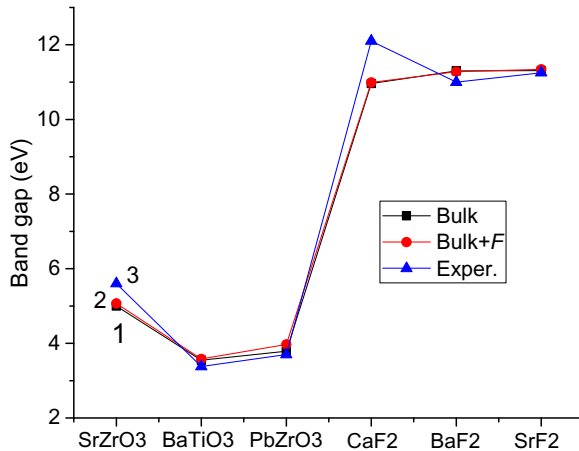


Fig. 5. (Color online) Our *ab initio* B3PW computed SrZrO₃, BaTiO₃, PbZrO₃, CaF₂, BaF₂ and SrF₂ direct bulk bandgap value (1), direct bulk bandgap value containing the single F-center defect (2) as well as the experimental Γ - Γ bandgap (3) (in eV).

measured direct CaF_2 bulk bandgap at Γ -point (12.1 eV Ref. 66) is for the CaF_2 fluoride (1.14 eV) (Table 2 and Fig. 5). In contrast, the difference between our *ab initio* B3PW computed SrF_2 bulk bandgap at Γ -point (11.31 eV) as well as the respective experimental bandgap (11.25 eV) is only 0.06 eV (Table 2). It is worth to note, that according to our *ab initio* B3PW computations, the F -center defect containing SrZrO_3 , BaTiO_3 , PbZrO_3 , CaF_2 and SrF_2 direct bulk bandgaps are slightly larger than the respective bulk bandgaps for the pristine materials (Table 2 and Fig. 5). The single exception from this systematic trend is our *ab initio* B3PW computed Γ - Γ bandgap for the perfect BaF_2 bulk (11.30 eV) (Table 2 and Fig. 5), which is 0.02 eV larger than the respective Γ - Γ bandgap for the BaF_2 fluoride containing the F -center defect. As a next step, we performed the relaxation of nearest neighbor atoms, surrounding the F -center defect in BaF_2 , SrF_2 and CaF_2 matrixes (Table 3). As we can see from Table 3, for all three our *ab initio* B3PW computed BaF_2 , SrF_2 and CaF_2 fluorides, the fluorine atom F is attracted towards the bulk F -center by (-0.23% , -0.27% and -0.28% of the a_0 , respectively). The displacement magnitudes of Ba, Sr and Ca atoms are considerable smaller ($+0.03\%$, -0.02% and $+0.15\%$ of a_0 , respectively). The Ba and Ca atoms are repulsed from the bulk F -center, whereas the Sr atom, by a very small magnitude (-0.02% of a_0), is attracted towards the SrF_2 fluoride bulk F -center (Table 3).

It is worth to note that in the case of the (111) surface F -center in the BaF_2 fluoride, the nearest neighbor atom displacement magnitudes are slightly larger than it was for the bulk F -center in the BaF_2 matrix (Table 3). Namely, the nearest Ba atoms are attracted towards the (111) surface F -center in the BaF_2 fluoride by (-0.13% of the a_0).

Also, the next nearest neighbor F atoms in BaF_2 are attracted towards the (111) surface F -center by approximately 1.5 times larger relaxation magnitude (-0.37% of a_0) than it was in the BaF_2 bulk F -center case (-0.23% of a_0) (Table 3).

As we can see from Table 4, the nearest neighbor B atoms always are repulsed from the bulk F -center in SrZrO_3 , PbZrO_3 , BaTiO_3 and SrTiO_3 matrixes.^{67–75} The B atom repulsion displacement magnitudes are quite different, ranging from only ($+0.48\%$ of a_0) in the PbZrO_3 perovskite till ($+7.76\%$ of a_0) in SrTiO_3 (Table 4). Just opposite, the second nearest neighbor O atoms, according to our *ab initio* B3PW

Table 3. Our *ab initio* B3PW computed relaxation of ten nearest atoms surrounding the bulk F -center defect in BaF_2 , SrF_2 and CaF_2 matrixes (in % of bulk lattice constant a_0).

Material	n th nearest	Atom	Number	B3PW Δz (%)
BaF_2	1	Ba	4	+0.03
	2	F	6	-0.23
SrF_2	1	Sr	4	-0.02
	2	F	6	-0.27
CaF_2	1	Ca	4	+0.15
	2	F	6	-0.28

Table 4. Our *ab initio* B3PW computed three nearest neighbor atom displacements around the bulk *F*-center located in the SrZrO₃, PbZrO₃, BaTiO₃ and SrTiO₃ matrixes (% of a_0).

Material	SrZrO ₃	PbZrO ₃	BaTiO ₃	SrTiO ₃
B atom displ.	+3.68	+0.48	+1.06	+7.76
O atom displ.	-2.63	—	-0.71	-7.79
A atom displ.	+0.46	-5.99	-0.08	+3.94

computations, always are attracted towards the bulk *F*-center. The largest O atom displacement magnitude, towards the bulk *F*-center, again is in the SrTiO₃ perovskite (-7.79% of a_0), whereas the smallest O atom displacement magnitude, this time is for the O atom in the BaTiO₃ perovskite, only (-0.71% of a_0) (Table 4). Finally, the third nearest neighbor A atom displacement directions and magnitudes are quite different (Table 4). The A atoms are attracted towards the PbZrO₃ and BaTiO₃ bulk *F*-center, whereas they are repulsed from the bulk *F*-center in the SrZrO₃ and SrTiO₃ matrixes (Table 4).

As we can see from Table 5, in most cases, the displacement magnitudes of three nearest neighbor atoms around the (001) surface *F*-center in ABO₃ perovskites are considerably larger than it was for the bulk *F*-center case (Table 4). For example, in the SrZrO₃ perovskite, the repulsion magnitudes of the Zr atoms from the (001) surface *F*-center (+9.17% of a_0) is 2.49 times larger than for the bulk *F*-center case (+3.68% of a_0) (Tables 4 and 5). Also, attraction magnitude of the O atom as well as repulsion magnitude of the Sr atom around the SrZrO₃ (001) surface center are 1.58 and 16.7 times larger, respectively, than around the SrZrO₃ bulk *F*-center (Tables 4 and 5). The single exception from this systematic trend is Ti atom repulsion from the BaTiO₃ (001) surface *F*-center, only (+0.1% of a_0) (Table 5), which is smaller, than the Ti atom repulsion from the *F*-center located in the BaTiO₃ perovskite bulk (+1.06% of a_0) (Table 4).

As we can see from Table 6, our *ab initio* B3PW computed charge inside the bulk *F*-center in SrZrO₃, PbZrO₃ and BaTiO₃ perovskites always are larger than inside the (001) surface *F*-center (Table 6). The largest charge difference is between the PbZrO₃ bulk *F*-center charge (-0.68*e*) and PbZrO₃ (001) surface *F*-center charge (-0.3*e*) equal to 0.38*e*. Just opposite, the smallest charge difference is between the

Table 5. Our *ab initio* B3PW computed three nearest neighbor atom displacements around the (001) surface *F*-center located in the SZO, PZO, BTO and STO (% of a_0).

Material	SZO	PZO	BTO	STO
B atom displ.	+9.17	+8.46	+0.1	+14.0
O atom displ.	-4.16	—	-1.4	-8.0
A atom displ.	+7.68	+11.97	+1.0	—

Table 6. Our *ab initio* B3PW computed charge inside the SZO, PZO, BTO and STO bulk and (001) surface *F*-center (in e).

Material	SZO	PZO	BTO	STO
Bulk <i>F</i> -center charge	-1.25	-0.68	-1.103	-1.10
<i>F</i> -center charge on (001) surface	-1.10	-0.3	-1.052	—
O atom net charge	-2.0	-2.0	-2.0	-2.0

BaTiO₃ bulk *F*-center charge ($-1.103e$) and BaTiO₃ (001) surface *F*-center charge ($-1.052e$) equal to only $0.051e$ (Table 6). As we can see from Table 7, approximately 80%, 85% and 75% of charge are localized inside the BaF₂, SrF₂ and CaF₂ bulk *F*-center, respectively. According to our performed *ab initio* B3PW computations, inside the *F*-center located on the BaF₂ (111) surface is localized slightly less charge, only $-0.79e$.

As we can see from Table 8 and Fig. 6, our *ab initio* B3PW computed direct bandgap values for SrZrO₃, BaTiO₃, SrTiO₃, PbZrO₃ perovskites, containing the *F*-center defect, are equal to 5.07, 3.58, 3.63 and 3.97 eV, respectively. Our *ab initio* B3PW computed Γ - Γ bandgap values for BaF₂, SrF₂ and CaF₂ fluorides, containing the *F*-center, are equal to 11.28, 11.34 and 10.99 eV, respectively. It is worth to note that the *F*-center induced defect level in the SrZrO₃, BaTiO₃ and SrTiO₃ perovskite bulk are located closer to the conduction band bottom, than to the valence band top. Namely, the *F*-center induced defect levels in SrZrO₃, BaTiO₃ and SrTiO₃ perovskite bulk are located 1.12, 0.23 and 0.69 eV below the CB bottom (Table 8 and Fig. 6). It is worth to note that the (001) surface *F*-center induced defect levels in the SrZrO₃, BaTiO₃ and SrTiO₃ perovskites, are located even closer to the CB bottom, than it was in the bulk case. Namely, the (001) surface *F*-center induced defect levels in SrZrO₃, BaTiO₃ and SrTiO₃ perovskites are located only 0.93, 0.07 and 0.25 eV,

Table 7. Our *ab initio* B3PW computed charge inside the BaF₂, SrF₂ and CaF₂ bulk and (111) surface *F*-center (in e).

Material	BaF ₂	SrF ₂	CaF ₂
Bulk <i>F</i> -center charge	-0.801	-0.848	-0.752
<i>F</i> -center charge on (111) surface	-0.790	—	—
F atom net charge	-1.0	-1.0	-1.0

Table 8. Our *ab initio* B3PW computed direct bulk bandgap for *F*-center containing BaF₂, SrF₂, CaF₂, SrZrO₃, BaTiO₃, SrTiO₃ and PbZrO₃ crystals as well as the *F*-center defect level induced position under the CB bottom (in eV).

Material	BaF ₂	SrF ₂	CaF ₂	SrZrO ₃	BaTiO ₃	SrTiO ₃	PbZrO ₃
Bulk bandgap with <i>F</i> -center	11.28	11.34	10.99	5.07	3.58	3.63	3.97
Bulk <i>F</i> -center under CB	4.27	3.67	4.24	1.12	0.23	0.69	1.72
Surface <i>F</i> -center under CB	—	—	—	0.93	0.07	0.25	2.58

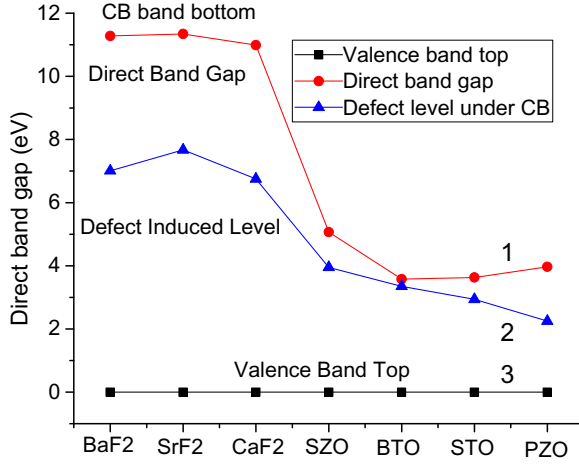


Fig. 6. (Color online) Our *ab initio* B3PW computed BaF₂, SrF₂, CaF₂, SrZrO₃, BaTiO₃, SrTiO₃, PbZrO₃ direct bulk bandgap values for crystal containing the *F*-center (1) (in eV). The *F*-center induced defect levels inside the bandgap (2) as well as the VB top (3).

respectively, below the CB bottom (Table 8). The single exception from this systematic trend is PbZrO₃ perovskite, where the situation is just opposite. Namely, in the PbZrO₃ perovskite, the bulk *F*-center induced defect level is located 1.72 eV below the CB bottom, whereas the (001) surface *F*-center induced defect level is located 2.58 eV below the CB bottom (Table 8). In the BaF₂, SrF₂ and CaF₂ fluoride bulk, the *F*-center induced defect level, is located 4.27, 3.67 and 4.24 eV, respectively, below the CB bottom (Table 8 and Fig. 6). Based on our *ab initio* B3PW computed defect levels in the BaF₂, SrF₂ and CaF₂ fluorides, we proposed the theoretical mechanism for explanation of the optical absorption experiment data in this three fluoride crystals.⁷⁶ Namely, we suggest that the experimentally observed optical absorption energy in BaF₂, SrF₂ and CaF₂ fluorides (2.3, 2.85, 3.3 eV, respectively) may be explained via the electron transfer from the *F*-center ground state, located (4.27, 3.67 and 4.24 eV, respectively) below the CB bottom, to the conduction band (Table 8 and Fig. 6). As we can see from Table 9 and Fig. 7, our *ab initio* B3PW computed BaF₂, SrZrO₃, BaTiO₃, SrTiO₃ and PbZrO₃ bulk *F*-center formation energies are equal to 7.82, 7.55, 10.3, 7.1 and 7.25 eV, respectively. In contrast, our *ab initio* computed surface *F*-center formation energies always are smaller (Table 9).

Table 9. Our *ab initio* B3PW computed *F*-center formation energies in BaF₂ bulk and on its (111) surface as well as in SrZrO₃, BaTiO₃, SrTiO₃ and PbZrO₃ perovskite bulk and on their (001) surfaces (in eV).

Material	BaF ₂	SrZrO ₃	BaTiO ₃	SrTiO ₃	PbZrO ₃
Material bulk	7.82	7.55	10.3	7.1	7.25
Surface	7.48	7.52	10.2	6.22	6.0

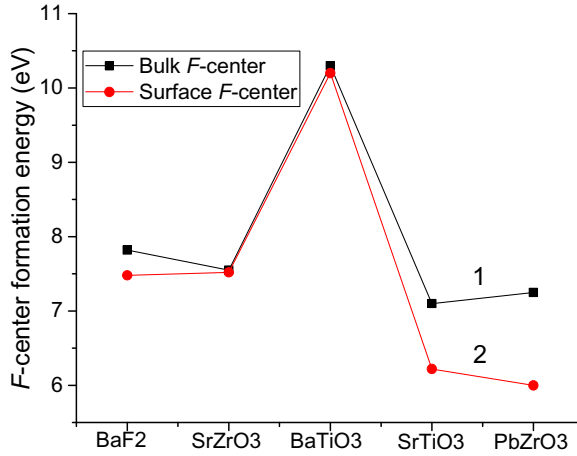


Fig. 7. (Color online) Our *ab initio* B3PW computed BaF₂, SrZrO₃, BaTiO₃, SrTiO₃, PbZrO₃ bulk (1) and surface (2) *F*-center formation energies (eV).

Namely, our *ab initio* B3PW computed *F*-center formation energy on BaF₂ (111) surface is equal to 7.48 eV, or by 0.34 eV smaller than it was in the BaF₂ bulk. Also, for SrZrO₃, BaTiO₃, SrTiO₃ and PbZrO₃ perovskites, our *ab initio* B3PW computed (001) surface energy (7.52, 10.2, 6.22 and 6.0 eV, respectively) is by (0.03, 0.1, 0.88 and 1.25 eV, respectively) smaller than it was in the bulk case (Table 9 and Fig. 7).

4. Conclusion

The displacement magnitudes of atoms, surrounding the (001) surface *F*-center in SrZrO₃, BaTiO₃, SrTiO₃ and PbZrO₃ perovskites, in most cases, are considerably larger than the respective displacement magnitudes of atoms surrounding the bulk *F*-center. As a rule, the B atoms in ABO₃ perovskites are repulsed from the bulk and (001) surface *F*-center, whereas the O atoms are attracted towards the *F*-center. The atomic displacement magnitudes of atoms around the *F*-center in ABO₃ perovskites are much larger, than the respective atomic displacement magnitudes around the *F*-center in BaF₂, SrF₂ and CaF₂ fluorides.

The *F*-center formation energy, located on the (001) surface of ABO₃ perovskites as well as the (111) surface of BaF₂, as a rule, is smaller than for the respective bulk *F*-centers. This slight energy distinction encourages the *F*-center segregation from the bulk of the ABO₃ perovskite and BaF₂ matrixes towards their (001) or (111) surfaces, respectively. In SrZrO₃, BaTiO₃, SrTiO₃ and PbZrO₃ perovskites as well as BaF₂, the electron charge is better localized inside the bulk than the surface *F*-center. The charge inside the *F*-center is much better localized for BaF₂, SrF₂ and CaF₂ fluorides than SrZrO₃, BaTiO₃, SrTiO₃ and PbTiO₃ perovskites.

Our *ab initio* B3PW computed direct bandgaps in pristine SrZrO₃, BaTiO₃, SrTiO₃, PbZrO₃ perovskites as well as BaF₂, SrF₂ and CaF₂ fluorides are in a fair


agreement with the available experimental data. In most cases, the introduction of the *F*-center defect, slightly increase their direct bandgap value. The ABO₃ complex oxide material (001) surface *F*-center generated defect levels, in most cases, are positioned nearer to the (001) surface conduction band (CB) bottom than the bulk *F*-center generated respective defect levels. We suggest that the experimentally observed optical absorption energy in BaF₂, SrF₂ and CaF₂ fluorides (2.3, 2.85, 3.3 eV, respectively) may be explained via the electron transfer from the *F*-center ground state, located at (4.27, 3.67 and 4.24 eV, respectively) below the CB bottom, to the conduction band.

Acknowledgments


We greatly acknowledge the financial support from Latvian Council of Science via Grant No. LZP-2020/1-0345. The Institute of Solid State Physics, University of Latvia, as the Centre of Excellence, has received funding from the European Unions Horizon 2020 Framework Programme H2020-WIDESPREAD01-2016-2017-Teaming Phase2 under Grant Agreement No. 739508, project CAMART-2. S.P.K. acknowledges support by the National Academy of Sciences of Ukraine (Project No. 0116U002067). S.P.K. thanks the Leibniz Foundation of the University of Leipzig for their support and hospitality during his visit.


ORCID


Roberts Eglitis  <https://orcid.org/0000-0002-8772-257X>

J. Purans  <https://orcid.org/0000-0002-0358-6479>

A. I. Popov  <https://orcid.org/0000-0003-2795-9361>

S. Piskunov  <https://orcid.org/0000-0002-8768-0736>

Ran Jia  <https://orcid.org/0000-0002-3722-1195>

S. P. Kruchinin  <https://orcid.org/0000-0002-0674-5826>

References

1. R. I. Eglitis and D. Vanderbilt, *Phys. Rev. B* **76** (2007) 155439.
2. X. J. Hu, Y. Yang, C. Hou and T. X. Liang, *J. Phys. Chem. C* **126** (2022) 517.
3. R. I. Eglitis, S. Piskunov, A. I. Popov, J. Purans, D. Bocharov and R. Jia, *Condens. Matter* **7** (2022) 70.
4. M. Zhong, W. Zeng, F. S. Liu and B. Tang, *Surf. Interface Anal.* **51** (2019) 1021.
5. S. Piskunov and R. I. Eglitis, *Solid State Ionics* **274** (2015) 29.
6. F. A. Celik, *Bull. Mater. Sci.* **45** (2022) 108.
7. M. Bilal, S. M. A. Abbas, M. Sluydts *et al.*, *Phys. Lett.* **408** (2021) 127469.
8. G. Borstel, R. I. Eglitis, E. A. Kotomin and E. Heifets, *Phys. Status Solidi B* **236** (2003) 253.
9. G. R. Portugal, S. F. Santos and J. T. Arantes, *Appl. Surf. Sci.* **502** (2020) 144206.
10. R. I. Eglitis, *Phys. Stat. Sol. B* **252** (2015) 635.
11. N. Sharma and K. Hernandi, *Catalysts* **12** (2022) 1619.

12. R. I. Eglitis, J. Kleperis, J. Purans, A. I. Popov and R. Jia, *J. Mater. Sci.* **55** (2020) 203.
13. H. J. Chun, Y. Lee, S. Kim, Y. Yoon, Y. Kim and S. C. Park, *Appl. Surf. Sci.* **578** (2022) 152018.
14. W. Jia, V. S. Vikhnin, H. Liu, S. Kapphan and R. Eglitis, *J. Lumin.* **83-84** (1999) 109.
15. M. G. Galloni, G. Cerrato, A. Giordana, E. Falleta and C. L. Bianchi, *Catalysts* **12** (2022) 804.
16. L. Grigorjeva, D. K. Millers, V. Pankratov, R. T. Williams, R. I. Eglitis, E. A. Kotomin and G. Borstel, *Solid State Commun.* **129** (2004) 691.
17. R. I. Eglitis, S. Piskunov and Y. F. Zhukovskii, *Phys. Status Solidi C* **13** (2016) 913.
18. M. Dawber, K. M. Rabe and J. F. Scott, *Rev. Mod. Phys.* **77** (2005) 1083.
19. Y. Si, H. Liu, H. Yu, X. Jiang and D. Sun, *Surf. Coating Technol.* **431** (2022) 128008.
20. W. Zhong, D. Vanderbilt and K. M. Rabe, *Phys. Rev. B* **52** (1995) 6301.
21. W. Zhong, D. Vanderbilt and K. M. Rabe, *Phys. Rev. Lett.* **73** (1994) 1861.
22. R. E. Cohen, *Nature* **358** (1992) 136.
23. X. Yu, S. Wang, X. Zhang, A. Qi, X. Qiao, Z. Liu, M. Wu and L. Li, *Nano Energy* **46** (2018) 29.
24. H. Lu, S. Glinsek, P. Buragohain, J. Iniguez and A. Gruverman, *Adv. Funct. Mater.* **30** (2020) 2003622.
25. S. Das, S. Som, C. Y. Yang, S. Chavhan and C. H. Lu, *Sci. Rep.* **6** (2016) 25787.
26. G. Cappellini, A. Bosin, G. Serra, J. Furthmüller and F. Bechstedt, *ACS Omega* **5** (2020) 13268.
27. M. Häfner and T. Bredow, *J. Phys. Chem. C* **125** (2021) 9085.
28. C. Wen and M. Lanz, *Appl. Phys. Rev.* **8** (2021) 021307.
29. J. Arends, *Phys. Status Solidi B* **7** (1964) 805.
30. I. Nepomnyashchikh, E. A. Radzabov and A. V. Egranov, *Radiat. Eff. Defects Solids* **157** (2002) 715.
31. B. C. Cavenett, W. Hayes, I. C. Hunter and A. M. Stoneham, *Proc. R. Soc. Lond. Ser. A* **309** (1969) 53.
32. M. Wright, B. V. Stefani, A. Soeriyadi, R. Basnet, C. Sun, W. Weigand, Z. Yu, Z. Holman, D. Macdonald and B. Hallam, *Phys. Stat. Solidi (RRL)* **15** (2021) 2100170.
33. N. Zhang, C. Gao and Y. Xiong, *J. Energy Chem.* **37** (2019) 43.
34. G. Song, S. Cong and Z. Zhao, *Chem. Sci.* **13** (2022) 1210.
35. H. Attariani, K. Momeni and K. Adkins, *ACS Omega* **2** (2017) 663.
36. J. H. Crawford, *Nucl. Instrum. Methods Phys. Res. B* **1** (1984) 159.
37. H. Shi, R. I. Eglitis and G. Borstel, *Phys. Rev. B* **72** (2005) 045109.
38. H. Shi, R. I. Eglitis and G. Borstel, *J. Phys.: Condens. Matter* **18** (2006) 8367.
39. R. Jia, H. Shi and G. Borstel, *Comput. Mater. Sci.* **43** (2008) 980.
40. W. Zhong and D. Vanderbilt, *Phys. Rev. B* **53** (1996) 5047.
41. M. Stengal, D. Vanderbilt and N. A. Spaldin, *Nat. Mater.* **8** (2009) 392.
42. K. Schmalzl, D. Strauch and H. Schober, *Phys. Rev. B* **68** (2003) 144301.
43. M. C. Oliveira, R. A. P. Ribeiro, E. Longo, M. R. D. Bomio, F. V. Motta and S. R. D. Lazaro, *Int. J. Quantum. Chem.* **120** (2020) e26054.
44. T. Matsuda, S. Yamanaka, K. Kurosaki and S. Kobayashi, *J. Alloys Compd.* **351** (2003) 43.
45. D. Ligny and P. Richet, *Phys. Rev. B* **53** (1996) 3013.
46. R. Dovesi, V. R. Saunders, C. Roetti, R. Orlando, C. M. Zicovich-Wilson, F. Pascale, B. Civalieri, K. Doll, N. M. Harrison, I. J. Bush et al., *CRYSTAL-2017 User Manual* (University of Torino: Torino, Italy, 2017).
47. J. P. Perdew and Y. Wang, *Phys. Rev. B* **33** (1986) 8800; *Erratum in Phys. Rev. B* **40** (1989) 3399.

48. J. P. Perdew and Y. Wang, *Phys. Rev. B* **45** (1992) 13244.
49. S. Piskunov, E. Heifets, R. I. Eglitis and G. Borstel, *Comput. Mater. Sci.* **29** (2004) 165.
50. H. J. Monkhorst and J. D. Pack, *Phys. Rev. B* **13** (1976) 5188.
51. R. I. Eglitis and S. Piskunov, *Comput. Condens. Matter* **7** (2016) 1.
52. R. Eglitis and S. P. Kruchinin, *Mod. Phys. Lett. B* **34** (2020) 2040057.
53. R. I. Eglitis, *Int. J. Mod. Phys. B* **28** (2014) 1430009.
54. R. I. Eglitis, E. A. Kotomin, A. I. Popov, S. P. Kruchinin and R. Jia, *Low Temp. Phys.* **48** (2022) 80.
55. R. I. Eglitis, J. Purans, A. I. Popov and R. Jia, *Symmetry* **13** (2021) 1920.
56. B. J. Kennedy, C. J. Howard and B. C. Chakoumakos, *Phys. Rev. B* **59** (1999) 4023.
57. K. H. Hellwege and A. M. Hellwege, *Landolt-Bornstein New Series* (Springer, Berlin, 1969).
58. S. Aoyagi, Y. Kuroiwa, A. Sawada, H. Tanaka, E. Nishibori, M. Takata and M. Sakata, *J. Phys. Soc. Japan* **71** (2002) 2353.
59. M. Sato, Y. Soejima, N. Ohama, A. Okazaki, H. J. Scheel and K. A. Müller, *Phase Trans.* **5** (1985) 207.
60. J. M. Leger, J. Haines, A. Atouf and O. Schulte, *Phys. Rev. B* **52** (1995) 13247.
61. W. Hayes, *Crystals with the Fluoride Structure* (Clarendon Press: Oxford, UK, 1974).
62. M. Nicolav, *J. Cryst. Growth* **218** (2000) 62.
63. Y. S. Lee, J. S. Lee, T. W. Noh, D. Y. Byun, K. S. Yamaura and E. Takayama-Muromachi, *Phys. Rev. B* **67** (2003) 113101.
64. S. H. Wemple, *Phys. Rev. B* **2** (1970) 2679.
65. J. Robertson, *J. Vacuum. Sci. Technol. B* **18** (2000) 1785.
66. G. W. Rubloff, *Phys. Rev. B* **5** (1972) 662.
67. J. Carrasco, F. Illas, N. Lopez, E. A. Kotomin, Y. F. Zhukovskii, R. A. Evarestov, Y. A. Mastrikov, S. Piskunov and J. Maier, *Phys. Rev. B* **73** (2006) 064106.
68. E. A. Kotomin, S. Piskunov, Y. F. Zhukovskii, R. I. Eglitis, A. Gopejenko and D. E. Ellis, *Phys. Chem. Chem. Phys.* **29** (2008) 4258.
69. Q. Ji, L. Bi, J. Zhang, H. Cao and X. S. Zhao, *Energy Environ. Sci.* **13** (2020) 1408.
70. R. B. Wexler, G. S. Gautam, E. B. Stechel and E. A. Carter, *J. Am. Chem. Soc.* **143** (2021) 13212.
71. H. Y. Su and K. Sun, *J. Mater. Sci.* **50** (2015) 1701.
72. E. A. Kotomin, A. I. Popov and R. I. Eglitis, *J. Phys.: Condens. Matter* **4** (1992) 5901.
73. W. J. Yin, S. H. Wei, M. M. Al-Jasim and Y. Yan, *Phys. Rev. B* **85** (2012) 201201(R).
74. J. Park, Y. N. Wu, W. A. Saidi, B. Chorpening and Y. Duan, *Phys. Chem. Chem. Phys.* **22** (2020) 27163.
75. M. Tyunina, O. Pacherova, T. Kocourek and A. Dejneka, *Sci. Rep.* **11** (2021) 15247.
76. H. Shi, L. Chang, R. Jia and R. I. Eglitis, *J. Phys. Chem. C* **116** (2012) 4832.